RF Computations with the Finite Integration Technique (FIT) and the Coupled S-Parameter Calculation (CSC)

(Invited Paper)

Ursula van Rienen, Hans-Walter Glock, Karsten Rothemund, Jacek Junak*
Institute of General Electrical Engineering, Rostock University D-18051 Rostock Germany

Abstract

This paper starts with a very brief review of FIT [1], [2] on triangular grids [3], [4]. Next, it reports about some recent features in FIT to minimize the geometrical error while keeping the number of grid points as small as possible. Finally, a method is introduced to compute scattering properties and/or resonant fields in complex rf structures by combination of domain decomposition with any available CEM tool. We denote this method as Coupled S-Parameter Calculation [5]. Some examples are presented underlining the power of the methods described.

I. Introduction

Simulating electromagnetic fields in rf components, users are interested in consistent codes that allow for a good geometrical discretization of the structure under study, reaching most accurate results while keeping the storage and computing time requirements as low as possible. Storage became cheaper and cheaper over the last decades and clock rates raised rapidly following Moore's law. Yet, in the course of rapid prototyping the demand to compute more and more complex structures grew with the same speed, at least. In the beginning of the eighties of the last century it was possible to run problems with about $10^3 - 10^4$ number of unknowns on main frames. At that time it was worth to put effort in more sophisticated grids than a usual Cartesian grid. As an example, we will describe an implementation based on FIT with a triangular-hexagonal grid pair. Meanwhile, after extensive studies it seems most practicable to use Cartesian grids with a so-called conformal approach to approximate material boundaries. In cases where very complex structures shall be studied or where parameter studies for parts of a structure shall be carried out a high geometrical resolution can be reached or much computing time can saved by using domain decomposition. One approach, described here, to receive results for the complete structure from single computations for sub-domains is called Coupled S-Parameter Calculation. This approach also allows to set up databases for typical sub-components and thus to reuse computational results. It is possible to combine analytical as well as 2D and/or 3D numerical computations. With this methodology total numbers of unknowns in the order of 10^7 and higher can be handled on usual workstations or small servers.

II. Finite Integration Technique (FIT)

The Finite Integration Technique yields an *exact* representation of Maxwell's equations in integral form on a grid duplet $(G, \tilde{G})$, denoted as *Maxwell-Grid-Equations*:

$$\begin{aligned} \mathbf{C}\widehat{\mathbf{e}} &= -\tfrac{\partial}{\partial t}\widehat{\widehat{\mathbf{b}}} & \mathbf{S}\widehat{\widehat{\mathbf{b}}} &= 0 \\ \widetilde{\mathbf{C}}\widehat{\mathbf{h}} &= \tfrac{\partial}{\partial t}\widehat{\widehat{\mathbf{d}}} + \widehat{\widehat{\mathbf{j}}} & \widetilde{\mathbf{S}}\widehat{\widehat{\mathbf{d}}} &= \mathbf{q} \end{aligned} \tag{1}$$

The operators $\mathbf{C}$, $\widetilde{\mathbf{C}}$, $\mathbf{S}$ and $\widetilde{\mathbf{S}}$ can be interpreted as discrete curl operators $\mathbf{C}, \widetilde{\mathbf{C}}$, discrete divergence $\mathbf{S}, \widetilde{\mathbf{S}}$ and discrete gradient operators $\mathbf{G} = -\widetilde{\mathbf{S}}^T, \widetilde{\mathbf{G}} = -\mathbf{S}^T$. The vectors $\widehat{\mathbf{e}}, \widehat{\mathbf{h}}$, etc. hold scalar state variables defined as field integrals along edges $L_i, \tilde{L}_i$ and across facets $A_i, \tilde{A}_i$, yielding the so-called *grid voltages* $\widehat{\mathbf{e}}, \widehat{\mathbf{h}}$ and *grid fluxes* $\widehat{\widehat{\mathbf{b}}}, \widehat{\widehat{\mathbf{d}}}, \widehat{\widehat{\mathbf{j}}}$ on the primary grid G and the dual grid $\widetilde{G}$, respectively:

$$\begin{aligned} \widehat{e}_i &= \textstyle\int_{L_i} \mathbf{E}\cdot d\mathbf{s}, & \widehat{\widehat{b}}_i &= \textstyle\int_{A_i} \mathbf{B}\cdot d\mathbf{A}, \\ \widehat{h}_i &= \textstyle\int_{\tilde{L}_i} \mathbf{H}\cdot d\mathbf{s}, & \widehat{\widehat{d}}_i &= \textstyle\int_{\tilde{A}_i} \mathbf{D}\cdot d\mathbf{A}, & \widehat{\widehat{j}}_i &= \textstyle\int_{\tilde{A}_i} \mathbf{J}\cdot d\mathbf{A}. \end{aligned} \tag{2}$$

The FIT grid duplet $(G, \widetilde{G})$ is not coordinate-bounded, not necessarily orthogonal, not necessarily regular.

A. Classical FIT on a Triangular Grid

Two decades ago, FIT with triangular primary grid was implemented in a program called URMEL-T [3]. The electric voltages are allocated on the triangular grid G and the magnetic voltages on the dual grid $\tilde{G}$ as in Fig. 1 or vice versa. Optimally, the mesh generator can set up a completely orthogonal dual grid $\tilde{G}_\perp$ composed of the perpendicular bisectors of the elementary lines L_i. Then, the intersections of the perpendicular bisectors, the circumcenters, give the dual grid points $\tilde{P}_i$. Its elementary

0-7803-7846-6/03/$17.00 ©2003 IEEE

areas $\tilde{A}_i$ in the grid plane are general hexagons, cf. Fig. 1. $\tilde{G}_\perp$ is a Delaunay-Voronoi mesh. For this dual-orthogonal FIT grid the continuity of tangential electric field and normal magnetic flux is preserved on all boundaries of different materials. Only if all triangles of the grid are acute or right-angled in the field carrying domain, $\tilde{P}_i$ lies inside the i-th triangle. Often, obtuse triangles occur near material boundaries. In that case the circumcenters are chosen for $\tilde{P}_i$ in all acute triangles and barycenters in the (usually very few) obtuse triangles. Then, the approximation order p is locally reduced to first order, overall p typically still has a value close (but smaller than) two.

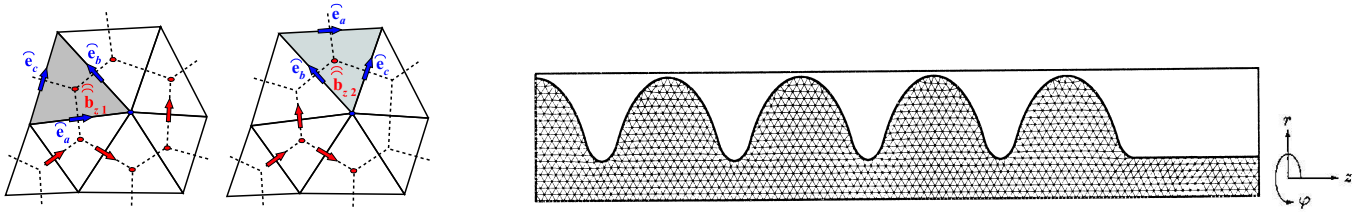

Fig. 1. Classical triangular FIT grid with its dual (hexagonal) grid, and some of the electric and magnetic state variables. The two kinds of primary cells are highlighted each. Right: Triangular grid for the right upper quarter of a cylindrically symmetric multicell rf resonator's cross section.

B. Conformal FIT

Since the numerical effort and the implementation effort for non-Cartesian grids is highly increased a diagonal filling of grid cells was used since long together with FIT. This already leads to much better and less oscillatory convergence as function of step size than the (still) usual FDTD staircase approximation. Yet, in order to reach an approximation order of two more sophisticated approaches are necessary. In [6] a strategy, now called Conformal FIT (CFIT), is introduced which - independently of the actual grid resolution - takes the actual material filling on boundaries into account when setting up the material matrices. It is implemented in CST Microwave Studio ®[7] used for the simulation displayed in Fig. 2. Thus, second order is reached allowing for rather accurate results even with rather coarse meshes. A simpler version of partially filled FIT cells was first introduced in [8] in context of some multigrid solver (cf. [9]).

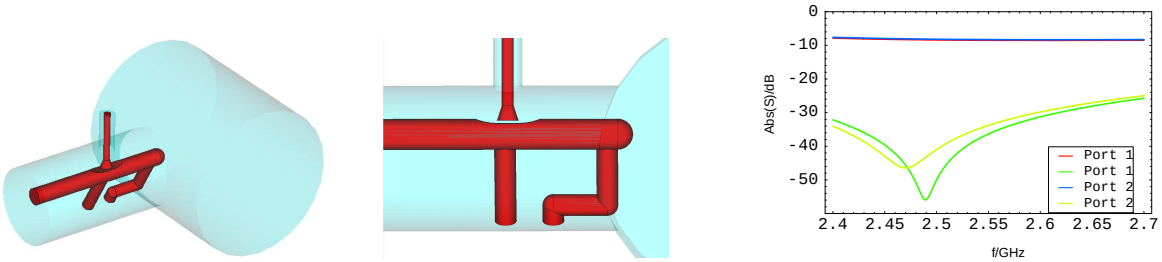

Fig. 2. Left: Geometry of coupler attached at the TESLA accelerating structure to damp parasitic higher order modes (HOMs). Middle: Detail. Right: S-parameters for signals between the coaxial port (top) and the beam pipe (right). Two polarization modes exist at each port.

III. Coupled S-Parameter Calculation (CSC)

Motivated by some previous work with the semi-analytical mode matching technique [10] we followed a similar approach of subdividing complex rf structures in simpler sub-objects for which the scattering parameters are computed either analytically or numerically, e.g. with available codes based on FIT. Herein, the S-parameters describe signal reflection and transmission between the n ports of a given rf-component. As standard, they are represented by an $(n\times n)$-matrix $\mathbf{S}$ where entry S_{ij} describes transmission of a signal from port j to port i. In general, it is a complex function of the frequency containing information about phase and amplitude. With $\mathbf{a}_k$ and $\mathbf{b}_k$ describing the input and output signals of the k-th sub-object, the matrix $\mathbf{S}_k$ forms the relation $\mathbf{b}_k = \mathbf{S}_k(\omega)\ \mathbf{a}_k$.

The $\mathbf{S}_k$ of all sub-objects are arranged in a block diagonal matrix $\mathbf{S}$ combining the vector $\mathbf{a}$ of all incident signals with vector $\mathbf{b}$ of all scattered signals, cf. also [11]:

$$\mathbf{b} = \mathbf{S}\,\mathbf{a} = \begin{pmatrix} \mathbf{S_1} & & \mathbf{0} \\ & \ddots & \\ \mathbf{0} & & \mathbf{S_N} \end{pmatrix} \begin{pmatrix} \mathbf{a}_1 \\ \vdots \\ \mathbf{a}_N \end{pmatrix} = \begin{pmatrix} \mathbf{b}_1 \\ \vdots \\ \mathbf{b}_N \end{pmatrix} \tag{3}$$

All signals incident in the full structure are collected in a vector $\mathbf{a}_{inc}$ whereas those signals travelling from one sub-object into a neighbouring one are grouped together in the coupling vector $\mathbf{a}_{cop}$. This reordering is done by a permutation matrix $\mathbf{P}$:

$$\mathbf{a} = \mathbf{P} \begin{pmatrix} \mathbf{a}_{cop} \\ \mathbf{a}_{inc} \end{pmatrix}. \tag{4}$$

The feedback inside the system, namely the fact that the outgoing signals of one port are incident signals at another port, is described by a feedback matrix $\mathbf{F}$; signals leaving the system are kept untouched. The inverse permutation ensures the same order of the scattered signals as in (4):

$$\begin{pmatrix} \mathbf{a}_{cop} \\ \mathbf{a}_{sct} \end{pmatrix} = \mathbf{P}^{-1}\,\mathbf{F}\,\mathbf{b}. \tag{5}$$

Combining (3), (4) and (5) results in the following matrix-vector-equation:

$$\begin{pmatrix} \mathbf{a}_{cop} \\ \mathbf{a}_{sct} \end{pmatrix} = \underbrace{\mathbf{P}^{-1}\,\mathbf{F}\,\mathbf{S}\,\mathbf{P}}_{\mathbf{G}} \begin{pmatrix} \mathbf{a}_{cop} \\ \mathbf{a}_{inc} \end{pmatrix}, \tag{6}$$

where $\mathbf{G} = \mathbf{P}^{-1}\,\mathbf{F}\,\mathbf{S}\,\mathbf{P}$ describes the structure of the whole system. $\mathbf{G}$ can be split into four block matrices $\mathbf{G}_{ij}$ according to the dimensions of $\mathbf{a}_{cop}$, $\mathbf{a}_{inc}$ and $\mathbf{a}_{sct}$. Thus, (6) can be written as the following system of matrix-vector-equations:

$$\mathbf{a}_{cop} = \mathbf{G}_{11}\,\mathbf{a}_{cop} + \mathbf{G}_{12}\,\mathbf{a}_{inc}, \tag{7a}$$

$$\mathbf{a}_{sct} = \mathbf{G}_{21}\,\mathbf{a}_{cop} + \mathbf{G}_{22}\,\mathbf{a}_{inc}. \tag{7b}$$

The coupling between the signals is then given by $\mathbf{a}_{sct} = \left(\mathbf{G}_{21}\,(\mathbf{1} - \mathbf{G}_{11})^{-1}\,\mathbf{G}_{12} + \mathbf{G}_{22}\right)\mathbf{a}_{inc}$. Because $\mathbf{a}_{inc}$ and $\mathbf{a}_{sct}$ represent the incident and reflected waves at the external ports

$$\mathbf{S}^{(TOT)} = \mathbf{G}_{21}\,(\mathbf{1} - \mathbf{G}_{11})^{-1}\,\mathbf{G}_{12} + \mathbf{G}_{22} \tag{8}$$

denotes the overall S-matrix $\mathbf{S}^{(TOT)}$ of the entire structure.

If all external ports are closed the structure becomes a resonator and only the coupling between the internal ports remains: $dim(\mathbf{a}_{sct}) = dim(\mathbf{a}_{inc}) = 0$. The block matrices $\mathbf{G}_{12}$, $\mathbf{G}_{21}$ and $\mathbf{G}_{22}$ vanish and (7) reduces to

$$(\mathbf{1} - \mathbf{G}_{11}(\omega_k))\,\mathbf{a}_{cop}^{(k)} = \mathbf{0}. \tag{9}$$

Eq. (9) is only fulfilled for a discrete spectrum of resonant frequencies ω_k with corresponding amplitude distributions $\mathbf{a}_k$. Their determination is explained in detail in [5].

IV. Example

As example, we regard a chain of slightly deformed cells of a multicell rf resonator like foreseen as superconducting accelerating structure in the TESLA project [12]. As more than 20,000 of those 9-cell resonators are foreseen for the high energy collider, the affordable tolerance is a major design criterion with various implications. One important point is the successful damping of parasitic higher order modes. In this context, we studied the effect of slightly elliptically deformed, twisted multicell structures with CSC. The single resonator cells were taken as sub-objects. It is sufficient to compute the S-parameters of the single (deformed) cells once, as long as we assume identical deformation for all cells. We used CST Microwave Studio ®[7] which is based on CFIT for the field simulation in the single cell.

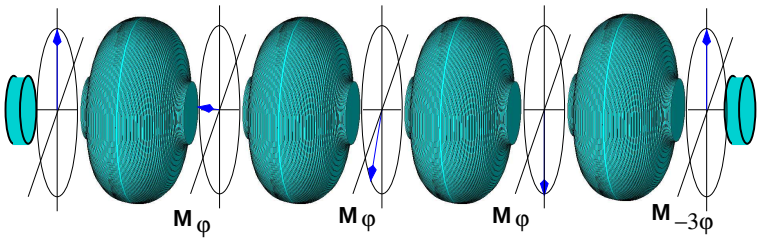

Fig. 3. Successive rotation of elliptically deformed TESLA-cells. Between the cells a vector indicates the local reference system; at the right end the reference system is rotated back to its original position.

The modeling of the rotation from one cell to the other is carried out introducing intermediate rotational objects (cf. Fig. 3). They represent a section of length zero rotating the reference plane by some angle φ:

$$\mathbf{M}_{\varphi} = \begin{pmatrix} 0 & 0 & \cos\varphi & \sin\varphi \\ 0 & 0 & -\sin\varphi & \cos\varphi \\ \cos\varphi & -\sin\varphi & 0 & 0 \\ \sin\varphi & \cos\varphi & 0 & 0 \end{pmatrix}. \tag{10}$$

In the following, we choose the angle φ to be identical for all cells. A rotation object with angle $\varphi_s = -(n-1)\,\varphi$ (n being the number of cells) is inserted between the last cell and the terminating short circuit in order to rotate the reference plane of the modes back to the initial reference system.

The rotation angle φ is varied in the range of $0 \ldots 90°$ in steps of $2°$. Figure 4 shows the resonant frequencies of a 4-cell resonator in the frequency range of $2.50 \ldots 2.57$ GHz. At $\varphi = 0°$ six separate modes, each in pairs, can be found. A degeneration of the polarization modes occurs at $\varphi = 90°$ such that only three resonant frequencies remain. The highlighted mode shows an additional degeneration at a rotation angle of about $50°$

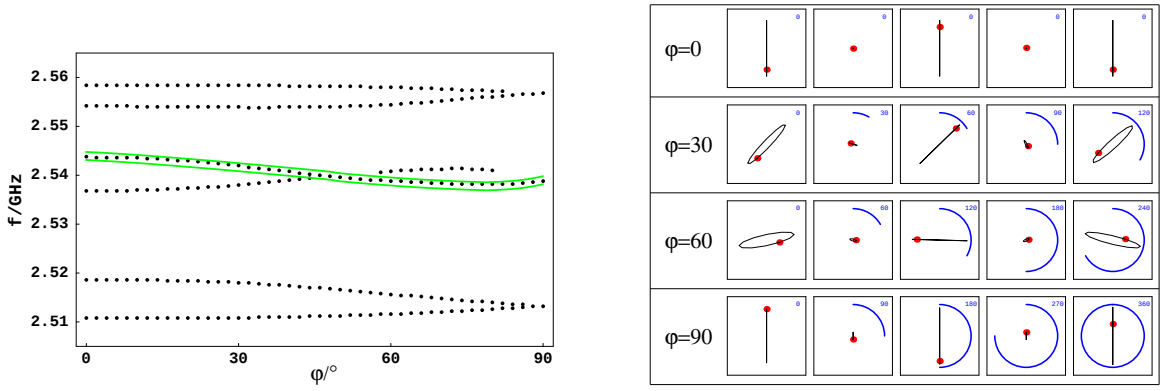

Fig. 4. Left: Resonant frequencies as function of the rotation angle φ. Especially highlighted is the frequency curve of mode no. 4 (related to $\varphi = 0°$). Right: Rotation in polarization of the **H**-field in the port planes of a 4-cell chain built from deformed TESLA cells. As example, mode 4 is chosen at angles 0, 30, 60 and $90°$ (cf. Fig. 3).

Besides the frequency shift of the eigenmodes the rotation of cells inside the resonator directly influences the field distribution of the modes. Figure 4 shows amplitude and orientation of the **H**-field of the highlighted mode in Fig. 3 - shown is a full period in the location of the port planes (left to right). Additionally, the start is marked by some point in order to better illustrate the phase relation of the signals. For $\varphi = 0°$, $|\mathbf{H}|$ has minima in port planes 2 and 4 and maxima in planes 1, 3 and 5. In plane 3, the field oscillates antiphase to the two outer ones. In all planes the mode shows linear polarization.

This basic form of the mode keeps unchanged if the rotation angle φ is varied. Yet, the field in planes 2 and 4 is no longer vanishing exactly. Additionally, for $\varphi = 30°$ and $60°$ the mode evidently shows an elliptic polarization in both outer port planes. For $\varphi = 60°$, a rotation of the principal ellipse axis can be observed, too. Both, elliptic polarization and rotation of polarization plane, can no longer be observed at $\varphi = 90°$ where, though, a non-vanishing field remains in the knot planes.

V. Conclusion

A variety of very reliable tools for electromagnetic field simulation based on the Finite Integration Technique, FIT, have been developed over the years. Their application range can successfully be further extended by use of the Coupled S-Parameter Calculation, CSC, allowing simulations for very complex rf structures by exploiting symmetries and repetitions of sub-objects.

Acknowledgment

The authors would like to thank Thomas Weiland and Martin Dohlus for many years of fruitful scientific cooperation and DESY (Deutsches Elektronen-Synchrotron), Hamburg, Germany, for continuous financial support.

References

[1] T. Weiland, "Eine Methode zur Lösung der Maxwellschen Gleichungen für sechskomponentige Felder auf diskreter Basis," *AEÜ*, vol. 31, pp. 116–120, 1977.
[2] ——, "Time Domain Electromagnetic Field Computation with Finite Difference Methods," *Int. Journal of Numerical Modelling: Electronic Networks, Devices and Fields*, vol. 9, no. 4, pp. 295–319, 1996.
[3] U. van Rienen and T. Weiland, "Triangular Discretization Method for the Evaluation of RF-Fields in Cylindrically Symmetric Cavities," *IEEE Transactions on Magnetics*, vol. 21, no. 6, pp. 2317–2320, November 1985.
[4] U. van Rienen, "Finite Integration Technique on Triangular Grids Revisited," *Int. Journal of Numerical Modelling: Electronic Networks, Devices and Fields, Special Issue "Finite Difference Time and Frequency Domain Methods"*, vol. 12, pp. 107–128, 1999, (invited paper).
[5] H.-W. Glock, K. Rothemund, and U. van Rienen, "Coupled Calculation of Eigenmodes," in *Computational Electromagnetics - Proceedings of the GAMM Workshop, Kiel, January 2001*, ser. Lecture Notes in Computational Science and Engineering, C. Carstensen, S. Funken, W. Hackbusch, R. H. Hoppe, and P. Monk, Eds., vol. 28. Springer Verlag, Berlin, 2003.
[6] B. Krietenstein, R. Schuhmann, P. Thoma, and T. Weiland, "The Perfect Boundary Approximation Technique Facing the Big Challenge of High Precision Field Computation," in *LINAC 98*, Chicago, USA, 1998, pp. 695–697, available: http://accelconf.web.cern.ch/AccelConf/l98/PAPERS/TH4041.PDF.
[7] CST - Computer Simulation Technology, Bad Nauheimer Str. 19, D-64289 Darmstadt, Germany.
[8] U. van Rienen and T. Weiland, "Impedance Calculation with URMEL-I Using Multigrid Methods," *IEEE, Trans. Magn.*, vol. 26, no. 2, p. 743, 1990.
[9] U. van Rienen, *Numerical Methods in Computational Electrodynamics - Linear Systems in Practical Applications*, ser. Lecture Notes in Computational Science and Engineering. Springer, 2001, vol. 12.
[10] ——, "Higher Order Mode Analysis of Tapered Disc-Loaded Waveguides Using the Mode Matching Technique," *Part.Acc.*, vol. 41, pp. 173–201, 1993.
[11] T.-A. Abele, "Über die Streumatrix allgemein zusammengeschalteter Mehrpole," *AEÜ*, vol. 14, pp. 262–268, 1960.
[12] R. Brinkmann, K. Flöttmann, J. Rossbach, P. Schmüser, N. Walker, and H. Weise, "TESLA - Technical Design Report, Part II," Deutsches Elektronen-Synchrotron DESY, D-22607 Hamburg, Germany, DESY 2001-011, March 2001, available: http://tesla.desy.de.